Published in final edited form as:
Neuron. 2010 February 11; 65(3): 399–411. doi:10.1016/j.neuron.2010.01.009.

Synaptic Inhibition in the Olfactory Bulb Accelerates Odor Discrimination in Mice

Nixon M. Abraham[1,2], **Veronica Egger**[3], **Derya R. Shimshek**[4], **Robert Renden**[1], **Izumi Fukunaga**[5], **Rolf Sprengel**[4], **Peter H. Seeburg**[4], **Matthias Klugmann**[6,&], **Troy W. Margrie**[7], **Andreas T. Schaefer**[2,5,7,#], and **Thomas Kuner**[1,2,#]

[1]Institute of Anatomy and Cell Biology, University of Heidelberg, INF 307, 69120 Heidelberg, Germany [2]WIN Olfactory Dynamics Group, Max Planck Institute for Medical Research, Jahnstrasse 29, 69120 Heidelberg, Germany [3]Institute of Physiology, LMU, Pettenkoferstr. 12, 80336 Munich [4]Dept. of Molecular Neurobiology, Max Planck Institute for Medical Research, Jahnstrasse 29, 69120 Heidelberg, Germany [5]SNWG Behavioral Neurophysiology, Max Planck Institute for Medical Research, Jahnstrasse 29, 69120 Heidelberg, Germany [6]Dept. of Molecular Medicine and Pathology, University of Auckland, Auckland, New Zealand [7]The Department of Neuroscience, Physiology and Pharmacology, University College London,The Rockefeller Building, 21 University Street, London, WC1E 6JJ, United Kingdom

Summary

Local inhibitory circuits are thought to shape neuronal information processing in the central nervous system, but it remains unclear how specific properties of inhibitory neuronal interactions translate into behavioral performance. In the olfactory bulb, inhibition of mitral/tufted cells via granule cells may contribute to odor discrimination behavior by refining neuronal representations of odors. Here we show that selective deletion of the AMPA receptor subunit GluA2 in granule cells boosted synaptic Ca^{2+} influx, increasing inhibition of mitral cells. On a behavioral level, discrimination of similar odor mixtures was accelerated while leaving learning and memory unaffected. In contrast, selective removal of NMDA receptors in granule cells slowed discrimination of similar odors. Our results demonstrate that inhibition of mitral cells controlled by granule cell glutamate receptors results in fast and accurate discrimination of similar odors. Thus, spatio-temporally defined molecular perturbations of olfactory bulb granule cells directly link stimulus-similarity, neuronal processing time and discrimination behavior to synaptic inhibition.

Introduction

When given enough time, rodents are capable of discriminating even highly similar olfactory stimuli with high accuracy (Abraham et al., 2004; Rinberg et al., 2006). However, when forced to make a rapid decision, accuracy is compromised (Rinberg et al., 2006; Uchida and

[#]Corresponding authors: Contact T. Kuner @ the University of Heidelberg for editorial correspondence: Tel. +49 6221-548678, Fax. +49 6221-544952, kuner@uni-heidelberg.de.
[&]Present address: Department of Physiological Chemistry, University of Mainz, Duesbergweg 6, 55099 Mainz, Germany.

Europe PMC Funders Author Manuscripts

Mainen, 2003). This phenomenon is widely known in sensory physiology and is referred to as the speed-accuracy tradeoff (Khan and Sobel, 2004; Luce, 1986). In fact, mice can discriminate simple odors with high accuracy in as little as 200 ms, but require 70-100 ms longer to accurately discriminate highly similar mixtures of the same odors (Abraham et al., 2004). The neuronal mechanisms acting during these additional tens of milliseconds of processing time, capable of resolving highly similar stimuli, remain unknown. Elucidating these mechanisms promises fundamental insights into how the olfactory system achieves fine odor discrimination.

The olfactory world is first represented at the level of the olfactory bulb (OB) as a spatiotemporal pattern of activity of functional units known as glomeruli (Reviewed by Mori et al., 1999; Kauer and White, 2001; Schaefer and Margrie, 2007). Mitral/tufted cells (here collectively referred to as mitral cells) both receive direct input from receptor neurons and also act as output cells of the OB (Shepherd and Greer, 1990), with tens of mitral cells being associated with a single glomerulus. Mitral cells receive projections of olfactory sensory neurons and extend their axons to different brain regions, prominently including the piriform cortex. They are synaptically coupled via inhibitory interneurons which are arranged in a two-stage network (Aungst et al., 2003). The OB circuitry is dominated by dendro-dendritic synapses formed between lateral dendrites of mitral cells and granule cells (GCs), the most numerous type of inhibitory axonless interneurons in the OB (Shepherd et al., 2007). Activation of a mitral cell will trigger dendritic release of glutamate onto synaptically coupled GCs, which in turn release gamma-aminobutyric acid (GABA) to inhibit the same as well as other mitral cells (Isaacson and Strowbridge, 1998; Jahr and Nicoll, 1980, 1982a, b; Mori et al., 1999; Nicoll, 1969; Nowycky et al., 1981; Phillips et al., 1963; Urban, 2002; Wellis and Kauer, 1993, 1994) This net-inhibition within and between mitral cells mediated by GCs plays a pivotal role in various hypotheses of odor representation and processing (reviewed in Cleland and Linster, 2005). It is thought to be crucial for synchronization and establishing slow temporal patterns in mitral cells (Laurent et al., 2001; Nusser et al., 2001; Schild, 1988). Inhibition might also enhance contrast in codes relying on the spatial representation of odors (Leon and Johnson, 2003; Mori et al., 1999; Schild, 1988; Urban, 2002; Yokoi et al., 1995) or sharpen activity onset (Margrie and Schaefer, 2003). Despite some understanding of the cellular mechanisms of inhibitory interactions between mitral and GCs, the contribution of inhibition to odor discrimination behavior has remained unresolved.

Synaptic interactions in the OB have been characterized at the cellular and molecular levels. For example, at the dendro-dendritic synapse, Ca^{2+} influx through ionotropic glutamate receptors (iGluR) on GCs can trigger the release of GABA and enhance inhibition of mitral cells (Chen et al., 2000; Halabisky et al., 2000; Isaacson, 2001). iGluRs of GCs are both of the fast AMPA and slow NMDA type (Montague and Greer, 1999; Sassoe-Pognetto and Ottersen, 2000). NMDA receptors containing the obligatory GluN1 subunit are highly Ca^{2+} permeable while AMPA receptors are rendered Ca^{2+} impermeable by the subunit GluA2 (previously referred to as GluR-B or GluR2) (Seeburg et al., 2001), which is expressed highly in the OB (Montague and Greer, 1999; Sassoe-Pognetto and Ottersen, 2000) and is functionally present in GCs at the dendro-dendritic synapse (Isaacson, 2001; Jardemark et al., 1997). Hence, we chose to selectively perturb iGluRs at the dendro-dendritic synapse and monitor the trace of such local perturbation through Ca^{2+} imaging, *in vitro* and *in vivo*

measurements of inhibition and odor discrimination behavior. Thus, using GC layer-specific perturbations of iGluRs we probed the neuronal mechanism of odor discrimination in mice.

Results

Granule cell-specific deletion of GluA2

To directly probe the contribution of the granule cell-mediated inhibition to odor discrimination, we targeted glutamate receptors on GCs. We first deleted the GluA2 subunit in GCs by viral expression of Cre recombinase in the OB of mice carrying conditional GluA2 alleles (*GluA2*^{2lox}) (Fig. 1A). Spatio-temporal control was achieved by stereotaxic delivery of recombinant adeno-associated virus encoding the Cre recombinase (AAV-Cre) into the GC layer (GCL) of the OBs of conditional GluA2 mice (Fig. 1B1). Anti-Cre stains of serially sectioned OB revealed that infected cells were almost exclusively found in the GC layer (Fig. 1B2, compare non-injected right OB with injected left OB). Only few Cre-expressing cells were present in the mitral cell layer (Fig. 1B3) and virtually no expression was found in the anterior olfactory nucleus, lateral olfactory tract and piriform cortex (Supplementary Figure S1). Five to six weeks after injection, almost half of the neurons in the GCL were infected (Fig. 1C). To assess the functionality of Cre-expression we quantified the amount of GluA2 by immunoblotting the total protein of the entire OB taken from mice at least five weeks after infection with AAV-Cre, the time required to complete the behavioral protocol used to determine odor discrimination times (ODTs, see below). The amount of GluA2 protein was decreased by almost 25% relative to control (Fig. 1D). This magnitude of reduction is consistent with the high abundance of GluA2 in the non-affected glomerular layer (Supplementary Figure S2A) and the expression of Cre recombinase in approximately 40% of the neurons in the GC layer. Notably, the amount of other AMPA receptor subunits such as GluA1 remained unchanged (Fig. 1D). A reduction of GluA2 in the GCL of *GluA2*^{2lox} mice injected with AAV-Cre was also detectable using immunohistochemistry (Supplementary Figure S2B). Hence, a significant number of GCs were infected, yielding a prominent and selective reduction of GluA2 expression predominantly in GCs of the OB.

Because deletion of GluA2 might affect synaptic interactions indirectly by altering cell morphology (Passafaro et al., 2003; Saglietti et al., 2007), we examined Cre-expressing and unperturbed GCs of *GluA2*^{2lox} mice. Granule cells lacking GluA2 did not show gross morphological alterations, with the number of spines per length of dendrite remaining unchanged (Supplementary Figure S3). Hence, the results demonstrate that AAV-mediated expression of Cre in mice with conditional GluA2 alleles resulted in a significant reduction of GluA2 expression in >40% of the GCs, while maintaining general GC morphology. We refer to mice such treated as *GluA2*$^{\Delta GCL}$.

Increased Ca^{2+} inflow into granule cells lacking *GluA2*

Removal of GluA2 from neurons has been shown to increase glutamate-mediated Ca^{2+} inflow in neuronal tissue outside the OB (Brusa et al., 1995; Feldmeyer et al., 1999; Jia et al., 1996). Together with Ca^{2+} entering through voltage-dependent Ca channels and Ca^{2+} released from internal stores (Egger et al., 2005), the resulting Ca^{2+}-load may modulate

GABA release (Chavez et al., 2006), with more Ca^{2+} causing increased GABA release and stronger inhibition of mitral cells (Chen et al., 2000; Halabisky et al., 2000; Isaacson, 2001; Isaacson and Strowbridge, 1998).

To test this, we compared Ca^{2+} transients elicited by glomerular stimulation in GC spines, also known as gemmules, of wild type and GluA2-depleted GCs. Simultaneous viral expression of Cre recombinase and Kusabira Orange (Tang et al., 2009) was used to identify GluA2-depleted GCs. Cells were patched with pipettes containing 100 μM OGB-1 and mitral cells were stimulated in the glomerular layer (Fig. 2A, Egger et al., 2005). The dendritic tree of electrically responsive GCs was scanned for gemmules producing postsynaptic Ca^{2+} transients (Fig. 2B). These transients were limited to the gemmule (Fig. 2B, grey versus black/red curves) and were not detectable in the adjacent dendritic shaft. The average ΔF/F amplitudes in control mice was 53 ± 42 % (n = 15 spines in 11 GCs). While the magnitude of the Ca^{2+} transients was within the same range in adult mice compared with our previous data from juvenile rats, we found a lower efficiency of synaptic transmission and a slower evolution of the spine Ca^{2+} signal in mice. The distribution of the individual synaptic events was irregular, with mostly smaller and a few large events, reflected in a median value of 33% and a skewness of 2.54 (Fig. 2C). In GluA2-depleted GCs, the average ΔF/F amplitude was 73 ± 17 % (n = 8 spines in 4 GCs), with the distribution of the individual events shifted to the right (Fig. 2B,C). Thus, GluA2-depleted GCs showed a significantly larger Ca^{2+} signal than wild type cells ($P < 0.01$, Mann-Whitney).

In summary, selective deletion of GluA2 in GCs increased synaptic Ca^{2+} transients in gemmules, the site of dendrodendritic communication.

Increased recurrent inhibition *in vivo*

The increased Ca^{2+} transient predicts an increased GABA release from the gemmule and thus stronger recurrent inhibition of mitral cells. To ensure anatomical integrity of the entire inhibitory network formed by GCs and mitral cells, we measured recurrent inhibition *in vivo* (Margrie et al., 2001) under ketamine/xylazine anesthesia (Fig. 3A). Whole-cell recordings were established from mitral cells of *GluA2*$^{\Delta FB}$ mice and littermate controls (see Methods for details). Neither average membrane potential (V_{cntrl}=-61.3±6.0 mV, n=9, V_{GluA2}=-54.6±4.0 mV, n=15, p=0.33, Mann-Whitney) nor cellular parameters such as input resistance (R_{cntrl}=54.3±10.5 MΩ, n=9, R_{GluA2}=62.2±6.4MΩ, n=15, p=0.61, Mann-Whitney) or time constant (τ_{cntrl}=7.1±1.1 ms, n=9, τ_{GluA2}=9.8±1.2, n=13, p=0.14, Mann-Whitney) nor sensory parameters such as oscillation amplitude (Margrie and Schaefer, 2003; A_{cntrl}=5.4±1.3 mV n=9, A_{GluA2}=4.4±0.9 mV, n=15, p=0.65, Mann-Whitney) or oscillation frequency (f_{cntrl}=3.0±0.8 Hz, n=9, f_{GluA2}=2.9±0.4 Hz, n=15, p=0.92, Mann-Whitney) were different, suggesting that the overall functionality of mitral cells as well as basic network properties were unaltered.

We then elicited 2-20 action potentials by brief current injections and recorded the hyperpolarizing response. As demonstrated before (Isaacson and Strowbridge, 1998; Jahr and Nicoll, 1982a; Margrie et al., 2001) this protocol elicits disynaptic recurrent inhibition as the evoked hyperpolarization is blocked by $GABA_A$ antagonists and blockers of

glutamatergic synaptic transmission, and reversed by increased intracellular chloride concentration (Fig. 3B, Isaacson and Strowbridge, 1998; Jahr and Nicoll, 1982a; Margrie et al., 2001). For 20 elicited action potentials, such recurrent IPSPs had an amplitude of 2.9±0.3 mV (n=9) in wild-type mice (Fig. 3C, D, black trace). Strikingly, *GluA2*$^{\Delta FB}$ mice showed a significantly increased recurrent IPSP of 4.2±0.4 mV (n=15, $p<0.05$, Mann-Whitney, Fig. 3C, D, red trace), further illustrated in the overlay of an average of all experiments in wild-type and *GluA2*$^{\Delta FB}$ mice (Fig. 3D). Because recurrent inhibition amplitudes could be strongly affected by local IPSP fluctuations we also analyzed the data by fitting the recurrent IPSP with an α-function template fit and by determining the integral of the IPSP (Supplementary Fig. S4). Both analyses yielded a substantial and highly significant difference between wild-type and *GluA2*$^{\Delta FB}$ mice (Fig. 3D, Supplementary Fig. S5). To assess the activity-dependence of recurrent inhibition, we quantified recurrent IPSPs evoked by 10, 5 and 2 APs as well. While the amplitude decreased with decreasing AP number, in virtually every case and for all three measures did GluA2 deletion result in a substantially increased IPSP magnitude (Fig. 3E). Therefore, GluA2 deletion from GCs caused a robust increase in recurrent inhibition in mitral cells in the intact network *in vivo*.

Increased recurrent inhibition *in vitro*

To exclude GC glutamatergic inputs arising from piriform cortex feedback or mitral cell axon collaterals, we repeated these experiments in isolated olfactory bulb slices from *GluA2*$^{\Delta GCL}$ mice. Figure 4 shows that the same protocol as used *in vivo* also resulted in hyperpolarization of mitral cells *in vitro*. To study the hyperpolarizing effect in detail, we also performed a series of pharmacological experiments in control mice. The response was blocked by gabazine (66.4±5.1% block, n=11 cells), APV (39.4±5.8% block, n=10 cells) as well as bath-loading of the membrane permeable Ca^{2+} chelator BAPTA-AM (61.2±5.2% block, n=12 cells) (Supplementary Fig. S6A,B), suggesting that the hyperpolarization reflects mostly recurrent inhibition (Isaacson and Strowbridge, 1998). Selective GluA2 ablation in GCs resulted in a significant increase in recurrent inhibition and decay time constant (Fig. 4B,C). This increase must be due to intrinsic bulbar circuits, because the slicing procedure removed all neuronal connections between the OB and cortex. Furthermore, in most of the recordings we found only a short axon, often ballooned at its severed end due to the slicing procedure (Supplementary Fig. S6C). This makes functional local recurrent axon projections targeting GCs connected to the same mitral cell highly unlikely. Therefore, consistent with the fact that the genetic manipulation did not affect mitral cells, these data demonstrate that recurrent inhibition mediated by the dendrodendritic synapse is increased in *GluA2*$^{\Delta GCL}$ mice.

Odor discrimination behavior of *GluA2*$^{\Delta GCL}$ *mice*

Having obtained a highly localized modification of olfactory bulb GCs resulting in increased Ca^{2+} influx in GC spines and consequently increased GC-mediated inhibition of mitral cells *in vitro* and *in vivo*, we are now in a position to investigate the behavioral consequences of such targeted alteration to the olfactory bulb inhibitory network.

We trained a cohort of mice on odor discrimination using go/no-go operant conditioning (Supplementary Fig. S7A, Abraham et al., 2004). To control for possible non-specific effects

of surgery, stereotaxic procedure or overexpression of Cre recombinase, we compared the *GluA2*$^{\Delta GCL}$ mice with two control groups: *GluA2*^{2lox} mice injected with PBS and C57BL6 mice injected with AAV-Cre.

Mice first learned to discriminate cineol (C) from eugenol (E) to become familiar with the olfactory operant conditioning task. After 1200 trials, mice could discriminate C from E with an accuracy of ~95% (Fig. 5A). Discrimination of a second simple odor pair amyl acetate (AA) and ethylbutyrate (EB) was readily accomplished thereafter reaching an accuracy of ~95%. Subsequently, mice learned to discriminate a difficult stimulus consisting of a binary mixture of AA and EB (60%AA+40%EB versus 40%AA+60%EB). Although >90% accuracy of discrimination was readily reached, mice needed longer training to reach this level (Abraham et al, 2004). These results were reproduced in a repetition of AA/EB simple and difficult discrimination tasks at the end of the experiment. In the final 300 trials of the simple and mixture discrimination (color coded bars), mice reached a saturating performance exceeding 95% accuracy (Fig. 5B). During the entire experiment, the intertrial interval was indistinguishable in all experimental groups (Supplementary Fig. S7B), suggesting comparable motivational conditions. Furthermore, learning curves were indistinguishable between the groups (Fig. 5A, $p>0.4$ for comparing the “normalized integration values” [NIV], Doucette et al., 2007, see Methods). Hence, both control and *GluA2*$^{\Delta GCL}$ mice could learn to discriminate simple odors and difficult mixtures equally well and with high accuracy.

Memory was tested after the first AA/EB episode (trials 1300 to 2400) by introducing another odor pair, pelargonic acid (Pel) versus valeric acid (Val). Again, mice acquired this task equally well than the preceding AA/EB task (Fig. 5A). During the final 140 Pel/Val trials, mice were intermittently challenged with discrimination of the C/E odor pair, which they had learned two weeks earlier (Shimshek et al, 2005). Both groups of mice remembered the previously learned odor pair in >80% with indistinguishable memory performance (Fig. 5C).

As described previously, olfactory discrimination times (ODTs) were determined for the final 300 trials, at a stage of stable performance (See Fig. 3,4 in (Abraham et al., 2004). The two control groups mentioned above did not show detectable differences [AA vs. EB: 227±14 ms in *GluRA2*^{2lox} mice injected with PBS (n=5), and 220±8 ms in *C57BL6* mice injected with AAV-Cre ($p=0.6$, n=8). Similar mixtures: 301±12 ms and 317±18 ms, respectively ($p=0.5$), Student *t*-test. Furtheron, control groups were pooled.], suggesting that neither Cre recombinase nor the stereotaxic injection influenced the performance. Strikingly, *GluA2*$^{\Delta GCL}$ mice discriminated the binary mixtures about 50 ms faster than control mice without significantly improving the discrimination of simple odors (Fig. 5D). At first glance, this 17% decrease in ODT appears to be a rather small change. In control animals, however, odor discrimination of highly similar stimuli required 70-100 ms longer than discrimination of simple odors. This additional temporal requirement is reduced by a factor of two in *GluA2*$^{\Delta GCL}$, indicating a substantial improvement of the processes crucial for the refinement of odor representations.

In conclusion, deletion of the GluA2 subunit in approximately 40% of the OB GCs yielded faster discrimination of highly similar mixtures with uncompromised accuracy. This gain-of-function phenotype was only evident in the task for similar odor mixtures, but not simple odors. Such a pattern would indeed be expected for a mechanism enhancing differences in highly similar odor representations by inhibitory synaptic interactions (Cleland and Linster, 2005; Laurent et al., 2001; Leon and Johnson, 2003; Margrie and Schaefer, 2003; Mori et al., 1999; Schild, 1988; Shepherd and Greer, 1990; Urban, 2002).

Granule cell-specific deletion of GluN1

After determining the cellular and behavioral consequences of deleting the GluA2 subunit in GCs of the OB, we set out to study the effects of removing the GluN1 subunit in GCs. This perturbation will reduce functional NMDARs, the only direct source of GluR-mediated synaptic Ca^{2+} influx in GCs containing a normal complement of GluA2 subunits. Deletion of the GluN1 subunit was achieved by viral expression of Cre recombinase in mice with conditional GluN1 alleles (*GluN1*^{2lox}) resulting in *GluN1*$^{\Delta GCL}$ mice (Fig. 6A). Again, the GC layer was homogeneously infected with AAV-Cre yielding an infection rate of approximately 45% (Fig. 6B), and only very few cells in the mitral cell layer expressed Cre recombinase. Quantitative immunoblotting showed that the amount of GluN1 subunit protein was reduced by 33% (Fig. 6C). Again, GluA1 expression remained unaffected, suggesting the absence of global compensatory effects on AMPA receptors.

Physiologically, synaptic responses to glomerular stimulation of mitral cells (Egger et al. 2005) could be elicited in both control and GluN1-deleted cells. GluN1-deleted cells rested at the same membrane potential as GCs from control animals (-82 ± 5 mV, n=9, vs -79 ± 3 mV, n=17, p>0.1). The decay half duration of evoked EPSPs was significantly accelerated in ΔGluN1 GCs compared to control (τ_{cntrl}=39.4±4.0 ms, n=7 vs τ_{GluN1}=23.9±4.9 ms, n=7, p<0.05) and uncorrelated to membrane potential (r^2<0.1, p>0.5), consistent with the ablation of the GluN1 subunit (Fig. 6D). To obtain further evidence for this we tested if the decay kinetics of the EPSPs in ΔGluN1 GCs was sensitive to APV. Because APV application would also affect glomerular stimulation and thereby occlude effects on the dendrodendritic synapse, we examined APV effects on spontaneous EPSPs. We found that sEPSPs were significantly faster in GCs with GluN1-deletion (19 ± 9 ms, n = 9 cells; P < 0.001 versus control: 35 ± 9 ms, n=10 cells, t-test; GluA2-deleted cells: 37 ± 11 ms, n=9 cells) and unaffected by bath application of the NMDAR antagonist APV (ratio NoDrug/APV=1.31±0.06 for control [n=7] vs 0.93±0.04 for ΔGluN1 [n=3]; p<0.002; Supplementary Figure 8). The robust contribution of NMDA currents to the EPSP at hyperpolarized potentials might be explained by a strong local depolarization of the spine independent of the membrane potential recorded at the soma of the neuron (Egger et al., 2005). Together, these results indicate a successful functional ablation of the slow NMDA receptor in GCs.

In 12 GC spines with deleted GluN1-subunits that responded to mitral cell activation, the average ΔF/F was reduced to 34 ± 10% (compare to 53 ± 42 % in control animals) and significantly less variable (absolute deviation from mean 10.0 ± 1.5 % compared to 23.7 ± 6.4 % in control animals, p<0.03). In particular, there were no large events, yielding a median value of 36%, a negligible skewness of - 0.10, and an 80th percentile of responses

that was reduced by half compared to control (52.4 ± 9.6% compared to 107.3 ± 54.5%, $p<0.03$, 1-tailed t-test). We estimate that the actual decrease in Ca^{2+} influx might be even larger, because ΔF/F values below 15% are generally not detectable. Finally, we recorded recurrent IPSP amplitudes in brain slices of *GluN1*$^{\Delta GCL}$ mice. Consistent with the accelerated EPSP and reduced Ca^{2+} influx in GCs, recurrent IPSPs of mitral cells showed a tendency to be reduced after GluN1-deletion compared to control (Fig. 6E).

Thus, while the physiological impact of GluN1 ablation is less pronounced than deletion of GluA2, the functional effect of GluN1 deletion was seen in alterations of EPSP kinetics and susceptibility to APV as well as in a reduced synaptic Ca^{2+} transient. Evoked recurrent IPSPs in the *GluN1*$^{\Delta GCL}$ mice displayed a trend opposite to the one found in *GluA2*$^{\Delta GCL}$ mice.

Following the same paradigm as described above for GluA2$^{\Delta GCL}$ mice, *GluN1*$^{\Delta GCL}$ and control mice readily acquired the simple and mixture discrimination tasks and achieved maximal discrimination accuracy (Fig. 7A,B). Overall learning performance was not significantly different between control and *GluN1*$^{\Delta GCL}$ mice (NIV, $p>0.2$, see Methods). Memory was not significantly affected (Fig. 7C). However, ODTs revealed an increase by about 60 ms in the mixture discrimination task without significantly altering the discrimination of simple odors, suggesting that NMDAR function at the dendro-dendritic synapse is essential for fast discrimination of similar odors (Fig. 7D).

Discussion

Our study took advantage of spatio-temporally defined deletions of iGluRs in GCs of the olfactory bulb by combining conditional gene deletion and viral expression of Cre recombinase. This approach facilitated the interpretation of behavioral results and allowed conclusions with respect to OB function unbiased by contributions of iGluR in other brain regions or during development. Deletion of iGluRs in GCs, the predominant inhibitory interneurons of the OB, resulted in bidirectional changes of odor discrimination time: *GluA2*$^{\Delta GCL}$ mice required ~50 ms less time (Fig. 8A, bold red line) than control mice (bold black line) to discriminate odor mixtures, while *GluN1*$^{\Delta GCL}$ mice needed ~60 ms longer (bold green line). These differences were only found in difficult discrimination tasks, consistent with the idea that inhibitory synaptic interactions improve discrimination of similar stimuli, but may not be needed to discriminate dissimilar stimuli (Fig. 8A, bold lines versus thin lines). Our *in vitro* and *in vivo* recordings from mitral cells of GluA2-deleted mice demonstrated that recurrent inhibition was markedly potentiated, suggesting that accelerated odor discrimination was caused by increased inhibition of mitral cells. While discrimination time changed bidirectionally, discrimination accuracy remained unaffected, suggesting that inhibitory interactions between mitral cells and GCs optimize speed-accuracy tradeoff such that the best possible decision can be secured in the fastest possible manner. We also found that learning of new tasks was not affected by deletion of iGluR in GCs, suggesting that at least subtle alterations of stimulus representations by inhibitory interactions between mitral cells and GCs are not necessary to support acquisition of a new discrimination task. Once mice had learned a task, deletions of iGluRs in GCs did not affect the retrieval of memories of previously learned tasks, while forebrain-specific deletion of

GluA2 promoted learning and decreased memory (Shimshek et al., 2005). These observations distinguish the main OB as the place of odor representation, encoding and primary processing, from higher order processing such as olfactory learning and memory predominantly taking place in downstream brain areas. In conclusion, our results provide a direct link between defined molecular perturbations, GC Ca^{2+} signals, synaptic inhibition, stimulus configuration and discrimination behavior mediated by the OB.

Granule cell-specificity of the molecular perturbations

Spatio-temporal control of gene deletion was achieved by stereotaxic injection of virus solution designed to infect the GC layer of the OB. Hence, geometry of the tissue and its demarcation to adjacent regions are important factors governing specificity. While this approach is not perfect, our injections were mostly limited to the GC layer of the OB with only few cells transduced outside this area. This specificity may simply be due to the geometry of the injection site or amplified by e.g. a glial sheath separating the granule cell layer from mitral cell layer.

The GC layer contains a heterogenous population of GCs, and also other, rarer neuronal cell types such as Blanes cells (Pressler and Strowbridge, 2006) or deep short axon cells (Eyre et al., 2009). However, their small number and mode of connectivity make the latter cells unlikely mediators of the altered inhibition onto mitral cells or the behavioral effects shown here.

Thus, our perturbations affected mostly GCs and hence we refer to the gene deletions performed in this study as ‘GC-specific’.

Cellular consequences of iGluR deletion in granule cells

Deleting the GluA2 subunit from GCs impacts glutamatergic transmission in several ways. First, Ca^{2+} permeability increases substantially, providing a stronger local glutamate-induced Ca^{2+} signal (Fig. 2). This may directly promote the release of GABA from synaptic vesicles adjacent to the postsynaptic density of the gemmule, and may therefore underlie a substantial portion of the increased recurrent IPSP (Fig. 3, 4). Second, the doubly-rectifying current-voltage relation of AMPA receptors devoid of GluA2 may generate a situation in which inflow of Na^{+} and Ca^{2+} will predominantly occur after periods of reduced activity, when the membrane potential is more strongly hyperpolarized. Third, the increased conductance of these receptors may result in stronger depolarization and therefore increased recruitment of voltage-gated Ca^{2+} channels, which in turn facilitates GABA release.

Beyond such considerations, an effect of GluA2 deletion on the recruitment of other AMPA receptor subunits and synapse morphology needs to be considered (Passafaro et al., 2003). However, we could not find any differences in GC morphology or number of spines *in vivo*, suggesting that the overall synaptic morphology was not affected by GluA2 deletion in GCs.

Deleting the GluN1 subunit from neurons results in a complete loss of functional NMDA receptors. Consequently, the predominant glutamate-mediated inflow pathway for direct synaptic Ca^{2+} will be abolished. In line with this, we found a reduction of synaptic Ca^{2+} events in $GluN1^{\Delta GCL}$ mice. Furthermore, the lack of NMDA receptor-mediated Na^{+} inflow,

which can be substantial in the physiological situation due to the activation of NMDA receptors for several hundred milliseconds, is predicted to result in a strongly shortened EPSPs (see e.g. Fig 6) and decreased depolarization of the GC. Subsequent activation of voltage-gated Ca^{2+} channels will be reduced resulting in a decrease of GABA release and reduced inhibition of the mitral cell.

In summary, Ca^{2+} entry and depolarization will be increased by deletion of GluA2 but decreased by deletion of GluN1. This will translate into a respective increase or a decrease of mitral cell inhibition. The former could be directly demonstrated by *in vitro* as well as *in vivo* recordings of the recurrent IPSP.

Synaptic inputs to granule cells originating from structures other than mitral cell dendrites

In addition to the glutamatergic input via the reciprocal synapse, at least two other sources of glutamatergic inputs exist onto GCs: collaterals of the mitral cell axon and numerous centrifugal projections (Balu et al., 2007). Both types of synaptic connections are preferentially situated closer to the soma of GCs and not necessarily adjacent to GABA release sites. Thus, for such glutamatergic inputs, deletion of GluA2 or GluN1 in GCs would potentially result in a modulation of global GC function, and thereby might gate the dendro-dendritic synapse (Balu et al., 2007). In our *in vivo* recordings, these connections could in principle contribute to the increased inhibition we observed. Their contribution, however, is unlikely to be substantial, as *in vitro* recordings clearly demonstrated that properties directly of the dendrodendritic synapse were altered: Ca^{2+} influx in GC gemmules was increased upon electrical stimulation in the glomerular layer and recurrent inhibition was increased after direct mitral cell stimulation. In both approaches, connections to higher order olfactory centers were disrupted and a majority of mitral cell axons were severed by the slicing procedure. Therefore, our data is consistent with the idea that ablation of iGluRs in the GCL significantly perturbed dendrodendritic inhibition via alterations in synaptic Ca^{2+} influx at the dendrodendritic synapse.

Local inhibitory synaptic interactions and processing time

Perturbations of iGluRs resulting in opposite cellular effects caused an increase or decrease in ODT of similar stimuli, while leaving the accuracy of odor discrimination as well as learning and memory unchanged (Figs. 5&7). Here, we measured GC-mediated inhibition onto mitral cells *in vitro* and *in vivo*, in the latter case maintaining full connectivity of mitral and GCs. Granule-cell mediated inhibition is a key player in a variety of models of odor processing (Cleland and Linster, 2005; Laurent et al., 2001; Leon and Johnson, 2003; Margrie and Schaefer, 2003; Mori et al., 1999; Nusser et al., 2001; Schild, 1988; Shepherd and Greer, 1990; Urban, 2002) and may thus represent the substrate of the stimulus-dependent changes in processing time described here. Therefore, we provide the first experimental evidence *in vivo* that iGluRs control inhibitory gain in the dendro-dendritic synapse and that such gain defines ODT in a bidirectional manner, with a larger gain resulting in stronger inhibition and faster discrimination.

Further support for a central role of inhibition arises from our observation that removal of GluA2 resulted in an accelerated ODT when mice discriminated highly similar odor

mixtures while remaining unchanged when mice discriminated simple odors. This pattern is consistent with the idea that simple odors produce distinct spatio-temporal patterns of activity (Abraham et al., 2004; Schaefer and Margrie, 2007; Spors and Grinvald, 2002) that can be readily distinguished with minimal processing by the olfactory system. In contrast, highly similar odor mixtures produce overlapping and highly similar activity patterns (Abraham et al., 2004), perhaps revealing a need for neuronal mechanisms of pattern separation as a prerequisite for accurate odor discrimination. Our results strongly suggest that inhibitory synaptic interactions between GCs and mitral cells can subserve this role. Based on our observations that ODT can be decreased by ~50 ms or increased by ~60 ms, we predict that the OB circuitry integrates and shapes odor-evoked excitation over such time periods, until the processed activity patterns are sufficiently different for neuronal networks downstream of the OB to yield highly accurate discrimination (Laurent et al., 2001).

The question remains how the molecular and cellular changes translate into increases or decreases of ODT in the range of tens of milliseconds. Assuming that inhibition has to reach a certain magnitude to affect early olfactory processing, this level would be reached approximately 50 ms faster in GluA2-deleted cells and approximately 70 ms slower in GluN1-deleted cells compared to control cells (Fig. 8B). Therefore, simply the speed of inhibition build-up in mitral cells, governed by the specific properties of the dendrodendritic synapse, may underlie shifts in ODT in the temporal range. Alternatively, increased or decreased inhibition might result in more, respectively less efficient spatiotemporal patterning, thus reducing or increasing the time needed to integrate in downstream structures.

Alterations of OB inhibitory interactions do not impact on learning and memory

The GC-specific deletion of iGluRs demonstrated a role of the OB in early processing of odor representations. Our previous work showed that deletion of GluA2 in the entire forebrain also resulted in accelerated learning but additionally impaired memory (Shimshek et al., 2005). The impaired memory was partially rescued by overexpression of GluA2 in the piriform cortex (Shimshek et al., 2005), whereas we show here that alterations restricted to OB GCs do not significantly impact on olfactory learning and memory.

Taken together, these results attribute to the OB an early processing role whereas the locus of memory is more likely, although not necessarily exclusively, the piriform cortex. Furthermore, the observed accelerated learning (Shimshek et al., 2005) cannot be solely attributed to the improved discrimination acuity but might involve contributions from higher forebrain areas.

Gain of function at which cost?

The gain-of-function phenotype described here prompts the question if other functions of the olfactory system are compromised instead. For instance, increased inhibition might result in a net loss of activity and thus a potentially reduced signal-to-noise relation for weak stimuli. It could therefore be speculated that detection thresholds for low odor concentrations or reaction times for detection of odors at low concentrations might be increased. Similarly,

more complex tasks such as foreground-background separation might suffer from suboptimal inhibition.

As rapid odor discrimination is a behavioral trait of high importance for survival, it seems likely that evolution would have eliminated GluA2 in GCs if there were no negative consequence associated with it. Nevertheless, this remains purely speculative until new quantitative behavioral tasks can be employed to identify these consequences.

Experimental procedures

Mice lines

GluA2(GluR-B)^{2lox}, *GluA2(GluR-B)*$^{\Delta FB}$ and *GluN1(NR1)*^{2lox} mice (previous nomenclature in parentheses, new nomenclature according to (Collingridge et al., 2009) were described previously (Shimshek et al., 2006; Shimshek et al., 2005).

Acute targeted genetic perturbation

The rAAV-Cre plasmid (Monory et al., 2006) contained the coding sequence for Cre recombinase, N-terminally fused to the hemagglutinin (HA)-tag and the SV40 nuclear localization signal in a rAAV plasmid backbone (pAM) containing the 1.1kb CMV enhancer/chicken ß-actin (CBA) promoter, the woodchuck post-transcriptional regulatory element (WPRE) and the bovine growth hormone polyA. For physiology experiments we used rAAV constructs containing iCre-2A-Venus (mitral cell recordings) and iCre-2A-KO (granule cell recordings and Ca^{2+} imaging, Tang et al., 2009)

rAAV chimeric vectors (virions containing a 1:1 ratio of AAV1 and AAV2 capsid proteins with AAV2 inverted terminal repeats) were generated as described (Klugmann et al., 2005). The genomic titer of the virus solution was $3.3x10^{12}$ particles/ml.

Stereotaxic injections were done as described in Wimmer et al., 2004, but using a BENCHMARK™ stereotaxic instrument (myNeurolab, St. Louis, USA). Mice (*C57BL6*, *GluA2*^{2lox} and *GluN12lox*) were injected at postnatal day 21 to 28. GCL-specific injection coordinates were found after a series of dye injections in the OB. Stereotaxic injection positions were defined relative to the center of the OB on the dorsal side of the OB. This center point was decided on the measurements of anterior-posterior and medio-lateral boundaries when viewing the OB from the dorsal side. The reproducibility of this center point across different animals was always monitored based on the relative position of this point with respect to bregma. At each of the four injection spots around 200 to 400 nl were injected. All experiments were conducted in accordance with the German animal welfare guidelines specified in the TierSchG.

Expression analysis

Immunohistochemistry and Western blots were performed as described (Shimshek et al., 2005). Details are described in the Supplemental Methods. Data are presented as mean ± SEM. Statistical significance was evaluated by two-tailed, unpaired student-*t* test.

Recording synaptic Ca^{2+} transients

Sagittal olfactory bulb brain slices (thickness 250 μm; P23-45) were prepared of wild type and $GluA2^{2lox}$ mice injected with AAV-Cre-2A-KO (Tang et al., 2009) to facilitate targeted patch-clamp recordings. Neurons were visualized using infrared gradient-contrast illumination and patched with pipettes having open tip resistances of 6-8 MΩ. Somatic whole-cell patch-clamp recordings were performed using an EPC-9 amplifier (HEKA, Lambrecht, Germany) following previously published procedures (Egger et al., 2003). Details are described in the Supplementary Methods.

To assess statistical significance levels, the nonparametric Wilcoxon matched-pairs signed-ranks test was applied for comparing paired data sets and the Mann-Whitney test for unpaired data; averages are given ± S.D., unless stated otherwise.

Recording recurrent inhibition *in vivo*

Whole-cell recordings were carried out on mitral cells of the OB of freely breathing mice anaesthetized with a ketamine (50 mg/kg)/xylazine (5 mg/kg) mixture as described previously (Margrie et al., 2001; Margrie and Schaefer, 2003; Schaefer et al., 2006). All electrophysiological experiments and analysis were performed blind with respect to the genotype of the animal. To avoid craniotomies and duratomies in the recording area, $GluA2^{\Delta FB}$ mice with a forebrain-specific deletion of GluA2 were used for *in vivo* patch-clamp recordings (Shimshek et al., 2005). GluA2-ablation in the OB is virtually identical in both $GluA2^{\Delta FB}$ mice and $GluA2^{\Delta GCL}$ mice (cf. Fig. 1 of this manuscript and Fig 4 of Shimshek et al., 2005).

Respiration was measured using a plethysmograph constructed from a piezoelectric strap wrapped around the thorax (Kent Scientific Corporation, Litchfield, CT, USA; (Margrie et al., 2001; Margrie and Schaefer, 2003; Schaefer et al., 2006). Patch pipettes had tip resistances of 4-8MΩ when filled with (in mM): K methansulfonate 130, HEPES 10, KCl 7, EGTA 0.05, $Na^{2\pm}$ATP 2, $Mg^{2\pm}$ATP 2, GTP 0.5, biocytin 0.4% pH 7.2 with KOH. Recordings were obtained from a total of 29 mitral cells (generally identified based on location [290±90μm depth], membrane potential [-57±17 mV; corrected for LJP of 9.3 mV], input resistance (59±30 MΩ; all mean±SD) and respiration-linked subthreshold oscillation [amplitude: 4.8 ± 3.6 mV, frequency 3.0±1.9 Hz]. DC current was injected to result in on average 0-1 APs per respiration cycle.

To elicit APs, short current pulses were injected, triggered on the respiration cycle. Hence, only a short baseline of 100 ms was measured before current injection to ensure a defined reproducible phase with respect to respiration. Action potentials (APs) were evoked by short (generally 3 ms) square current injections with an interpulse interval of 8 ms.

Drugs (Gabazine, 500 μM; AP5, 500 μM, NBQX, 500 μM) were superfused over the exposed OB surface using a peristaltic pump (Ismatec, Glattbrugg, Switzerland) driven perfusion system.

Data analysis is described in detail in the supplementary information.

Recording recurrent inhibition *in vitro*

Horizontal olfactory bulb slices (300 μm thick) were prepared from P40-70 mice [GluA2$^{\Delta GCL}$, n=21, GluN1$^{\Delta GCL}$, n=19, C57 BL6, n=5, Controls, n=26 (GluA2 conditional KO littermates=21, GluN1 conditional KO littermates=5)] on a vibratome while submerged in ice-cold oxygenated sucrose-based Ringer solution containing (mM): NaCl 85, KCl 2.5, NaHCO3 25, NaH2PO4 1.25, Sucrose 75, MgCl2 3.3, CaCl2 0.5, glucose 25, ascorbate 0.4, pyruvate 2, myo-inositol 3. Slices were transferred to a warm (37 °C) oxygenated incubating bath for 30 min and then allowed to equilibrate to room temperature before being transferred to the recording chamber. Extracellular artificial cerebrospinal fluid was bubbled with carbogen and contained [mM]: NaCl 125, KCl 2.5, NaHCO3 25, NaH2PO4 1.25, MgCl2 1, CaCl2 2, glucose 25. All experiments were performed at temperatures between 23-26°C.

Electrophysiological recordings were done as described previously (Wimmer et al., 2004). Whole-cell recordings were established using an EPC9 and EPC10 patch-clamp amplifier (HEKA, Lambrecht, Germany) and pipettes with resistances of 4–6 MΩ filled with a solution containing (mM): potassium gluconate 135, Hepes 10, sodium phosphocreatine 10, MgATP 4, KCl 4, Na3GTP 0.3 (adjusted to pH 7.2 with KOH). The fluorescent dye Alexa 594 hydrazide (20 mM, Invitrogen, Molecular Probes, Oregon, USA) was included routinely in the intracellular solution to allow for morphological analysis. Action potentials (APs) were evoked by short (generally 3 ms) square current injections with an interpulse interval of 8 ms. Drugs used were D-Aminophosphonovalerate (APV, 50 μM, Ascent Scientific, New Jersey, USA), GABAzine (SR95531, 20 μM Ascent Scientific, New Jersey, USA), and BAPTA-AM (100 μM, Sigma-Aldrich Chemie GmbH, Steinheim, Germany). All procedures were performed according to the guidelines of the german animal welfare law.

Behavioral Training

Behavioral training started one week after surgery and was executed as described (Abraham et al., 2004; Shimshek et al., 2005). In all cases, the experimenter was blind with respect to the genotype (*GluA2*^{2lox} or *C57BL6*) and the injection state (PBS or AAV-Cre). One to two days prior to pre-training, mice were kept with restricted water access, and body weight was closely monitored and maintained >85% of their ad lib body weight. Continuous water restriction was never longer than 12 hrs.

Mice were trained on the discrimination task cineol (Cin) versus eugenol (Eu) for 1300 trials. Subsequently, the animals were trained for 600 trials on the “simple” odor pair (1% amyl acetate (AA) versus 1% ethyl butyrate (EB), and 600 trials of “difficult” odor pairs (mixtures of AA and EB with very similar ratio, 0.6% AA+0.4% EB v/s 0.4% AA+0.6% EB, Abraham et al., 2004). Subsequently, animals were trained for another simple odor task with different odors (Pelargonic vs Valeric acid) for 800 trials. During the last 140 trials of these 800 trails the memory for Cin vs Eu was measured (see the details below). This was followed by repetitions of the difficult (600 trials) and simple odor task (300 trials) with AA and EB to ensure stability of DT measurements (Abraham et al., 2004). At the end of the training, the animals were sacrificed and used for immunohistochemical analysis of Cre and western blot analysis of GluA1, GluA2 and GluN1.

Learning curves were analysed using the “normalized integration value” (NIV, Doucette et al., 2007). For GluA2, no effect of genotype [$F(1,22)=0.3$, $p>0.5$] and no interaction effect genotype x odor pair [$F(6,132)=0.4$, $p>0.8$] were found (two-way ANOVA with repeated measures). Comparison of NIVs for each odor pair separately showed $p>0.4$ for all odors (Student t-test). For GluN1, no effect of genotype [$F(1,17)=1.3$, $p>0.2$] and no interaction effect genotype x odor pair [$F(6,102)=1.1$, $p>0.3$] were found. Comparison of NIVs for each odor pair separately showed $p>0.1$ for all odors except for the first mixture training ($p=0.07$).

Memory was measured as described in Shimshek et al., 2005: In brief, during the last 100 trials of Cin vs Eu training only 50% of the S+ trials were rewarded in order to minimize extinction of the acquired memory during the subsequent testing task. These trials were excluded for the statistical analysis of learning curves. To assess memory, individual Cin and Eu trials were interleaved for the last 140 trials of Pel versus Val training, such that two unrewarded Cin and two unrewarded Eu trials were included in each block of 20 trials. Memory scores reflect the percentage of correct responses (licking response to the odor that was rewarded in the initial training session [S+], no response to the odor that was not rewarded initially [S-]).

Odor discrimination times (ODTs) were measured as described (Abraham et al., 2004). In brief, an individual trial is shown in Supplementary Figure S7: A trial is initiated by breaking a light beam at the sampling port opening. This opens one of eight odor valves and a diversion valve (DV) that allows all airflow to be diverted away from the animal for 500 ms. After the release of the DV, the odor is applied to the animal for 2 s. If the mouse continuously licks at the lick port during this time (once in at least three out of four 500 ms bins), it can receive a 4 μl water reward after the end of the 2 s period. If the animal does not continuously lick or if the presented odor was an S- odor no reward is supplied. Odors are presented in a pseudorandomized scheme (no more than two successive presentations of the same odor.

Upon presentation of a S+ odor, the animal generally continuously breaks the beam, whereas upon presentation of an S- odor an animal familiar with the apparatus usually quickly retracts its head. ODTs were calculated as follows: For every time point, beam breakings for S+ and S- odors were compared by bootstrapping, yielding a significance value as a function of time after odor onset. The last crossing of the $p = 0.05$ line determined the discrimination time (DT). In very few cases, this did not coincide with the visually identified discrimination time [point of largest curvature in the log(p)-t plot] and was corrected after visual inspection.

Supplementary Material

Refer to Web version on PubMed Central for supplementary material.

Acknowledgements

We thank Bert Sakmann for generous support and hosting the WIN Olfactory Dynamics Group during the initial part of the project, Hartwig Spors for discussions and comments on earlier versions of the manuscript, Tansu Celikel for discussions, Bhavana Shrivastava for help with morphological analysis, Olga Stroh for performing some of the electrophysiological recordings in granule cells, Heinz Horstmann, Michaela Kaiser, Claudia Kocksch for technical assistance, Thorsten Bus for pilot experiments and help with breeding mice and Kevin Martin for

comments. This work was supported by the Heidelberger Akademie der Wissenschaften, a Medical Faculty of the University of Heidelberg Postdoctoral Fellowship, the Leopoldina Akademie der Naturforscher, EMBO, the Bauer-Foundation, the BBSRC, the DFG (research grant KU1983/2 (FOR 643)) and the Max-Planck-Gesellschaft. PHS, ATS and TK are members of the CellNetworks - Cluster of Excellence (EXC81).

References

Abraham NM, Spors H, Carleton A, Margrie TW, Kuner T, Schaefer AT. Maintaining accuracy at the expense of speed: stimulus similarity defines odor discrimination time in mice. Neuron. 2004; 44:865–876. [PubMed: 15572116]

Aungst JL, Heyward PM, Puche AC, Karnup SV, Hayar A, Szabo G, Shipley MT. Centre-surround inhibition among olfactory bulb glomeruli. Nature. 2003; 426:623–629. [PubMed: 14668854]

Balu R, Pressler RT, Strowbridge BW. Multiple modes of synaptic excitation of olfactory bulb granule cells. J Neurosci. 2007; 27:5621–5632. [PubMed: 17522307]

Brusa R, Zimmermann F, Koh DS, Feldmeyer D, Gass P, Seeburg PH, Sprengel R. Early-onset epilepsy and postnatal lethality associated with an editing-deficient GluR-B allele in mice. Science. 1995; 270:1677–1680. [PubMed: 7502080]

Chavez AE, Singer JH, Diamond JS. Fast neurotransmitter release triggered by Ca influx through AMPA-type glutamate receptors. Nature. 2006; 443:705–708. [PubMed: 17036006]

Chen WR, Xiong W, Shepherd GM. Analysis of relations between NMDA receptors and GABA release at olfactory bulb reciprocal synapses. Neuron. 2000; 25:625–633. [PubMed: 10774730]

Cleland TA, Linster C. Computation in the olfactory system. Chem Senses. 2005; 30:801–813. [PubMed: 16267161]

Collingridge GL, Olsen RW, Peters J, Spedding M. A nomenclature for ligand-gated ion channels. Neuropharmacology. 2009; 56:2–5. [PubMed: 18655795]

Doucette W, Milder J, Restrepo D. Adrenergic modulation of olfactory bulb circuitry affects odor discrimination. Learning & Memory. 2007; 14:539–547. [PubMed: 17686948]

Egger V, Svoboda K, Mainen ZF. Mechanisms of lateral inhibition in the olfactory bulb: efficiency and modulation of spike-evoked calcium influx into granule cells. J Neurosci. 2003; 23:7551–7558. [PubMed: 12930793]

Egger V, Svoboda K, Mainen ZF. Dendrodendritic synaptic signals in olfactory bulb granule cells: local spine boost and global low-threshold spike. J Neurosci. 2005; 25:3521–3530. [PubMed: 15814782]

Eyre MD, Kerti K, Nusser Z. Molecular diversity of deep short-axon cells of the rat main olfactory bulb. The European journal of neuroscience. 2009; 29:1397–1407. [PubMed: 19344330]

Feldmeyer D, Kask K, Brusa R, Kornau HC, Kolhekar R, Rozov A, Burnashev N, Jensen V, Hvalby O, Sprengel R, Seeburg PH. Neurological dysfunctions in mice expressing different levels of the Q/R site-unedited AMPAR subunit GluR-B. Nat Neurosci. 1999; 2:57–64. [PubMed: 10195181]

Halabisky B, Friedman D, Radojicic M, Strowbridge BW. Calcium influx through NMDA receptors directly evokes GABA release in olfactory bulb granule cells. J Neurosci. 2000; 20:5124–5134. [PubMed: 10864969]

Isaacson JS. Mechanisms governing dendritic gamma-aminobutyric acid (GABA) release in the rat olfactory bulb. Proc Natl Acad Sci U S A. 2001; 98:337–342. [PubMed: 11120892]

Isaacson JS, Strowbridge BW. Olfactory reciprocal synapses: dendritic signaling in the CNS. Neuron. 1998; 20:749–761. [PubMed: 9581766]

Jahr CE, Nicoll RA. Dendrodendritic inhibition: demonstration with intracellular recording. Science (New York, N.Y. 1980; 207:1473–1475.

Jahr CE, Nicoll RA. An intracellular analysis of dendrodendritic inhibition in the turtle in vitro olfactory bulb. The Journal of physiology. 1982a; 326:213–234. [PubMed: 7108788]

Jahr CE, Nicoll RA. Noradrenergic modulation of dendrodendritic inhibition in the olfactory bulb. Nature. 1982b; 297:227–229. [PubMed: 7078637]

Jardemark K, Nilsson M, Muyderman H, Jacobson I. Ca2+ ion permeability properties of (R,S) alpha-amino-3-hydroxy-5-methyl-4-isoxazolepropionate (AMPA) receptors in isolated interneurons from the olfactory bulb of the rat. Journal of neurophysiology. 1997; 77:702–708. [PubMed: 9065842]

Jia Z, Agopyan N, Miu P, Xiong Z, Henderson J, Gerlai R, Taverna FA, Velumian A, MacDonald J, Carlen P, et al. Enhanced LTP in mice deficient in the AMPA receptor GluR2. Neuron. 1996; 17:945–956. [PubMed: 8938126]

Khan RM, Sobel N. Neural processing at the speed of smell. Neuron. 2004; 44:744–747. [PubMed: 15572105]

Klugmann M, Symes CW, Leichtlein CB, Klaussner BK, Dunning J, Fong D, Young D, During MJ. AAV-mediated hippocampal expression of short and long Homer 1 proteins differentially affect cognition and seizure activity in adult rats. Mol Cell Neurosci. 2005; 28:347–360. [PubMed: 15691715]

Laurent G, Stopfer M, Friedrich RW, Rabinovich MI, Volkovskii A, Abarbanel HD. Odor encoding as an active, dynamical process: experiments, computation, and theory. Annu Rev Neurosci. 2001; 24:263–297. [PubMed: 11283312]

Leon M, Johnson BA. Olfactory coding in the mammalian olfactory bulb. Brain Res Brain Res Rev. 2003; 42:23–32. [PubMed: 12668289]

Luce, RD. Response Times. Oxford: Oxford University Press; 1986.

Margrie TW, Sakmann B, Urban NN. Action potential propagation in mitral cell lateral dendrites is decremental and controls recurrent and lateral inhibition in the mammalian olfactory bulb. Proc Natl Acad Sci U S A. 2001; 98:319–324. [PubMed: 11120888]

Margrie TW, Schaefer AT. Theta oscillation coupled spike latencies yield computational vigour in a mammalian sensory system. J Physiol. 2003; 546:363–374. [PubMed: 12527724]

Monory K, Massa F, Egertova M, Eder M, Blaudzun H, Westenbroek R, Kelsch W, Jacob W, Marsch R, Ekker M, et al. The endocannabinoid system controls key epileptogenic circuits in the hippocampus. Neuron. 2006; 51:455–466. [PubMed: 16908411]

Montague AA, Greer CA. Differential distribution of ionotropic glutamate receptor subunits in the rat olfactory bulb. J Comp Neurol. 1999; 405:233–246. [PubMed: 10023812]

Mori K, Nagao H, Yoshihara Y. The olfactory bulb: coding and processing of odor molecule information. Science. 1999; 286:711–715. [PubMed: 10531048]

Nicoll RA. Inhibitory mechanisms in the rabbit olfactory bulb: dendrodendritic mechanisms. Brain research. 1969; 14:157–172. [PubMed: 5783107]

Nowycky MC, Mori K, Shepherd GM. GABAergic mechanisms of dendrodendritic synapses in isolated turtle olfactory bulb. Journal of neurophysiology. 1981; 46:639–648. [PubMed: 7299438]

Nusser Z, Kay LM, Laurent G, Homanics GE, Mody I. Disruption of GABA(A) receptors on GABAergic interneurons leads to increased oscillatory power in the olfactory bulb network. J Neurophysiol. 2001; 86:2823–2833. [PubMed: 11731539]

Passafaro M, Nakagawa T, Sala C, Sheng M. Induction of dendritic spines by an extracellular domain of AMPA receptor subunit GluR2. Nature. 2003; 424:677–681. [PubMed: 12904794]

Phillips CG, Powell TP, Shepherd GM. Responses of Mitral Cells to Stimulation of the Lateral Olfactory Tract in the Rabbit. The Journal of physiology. 1963; 168:65–88. [PubMed: 14056493]

Pressler RT, Strowbridge BW. Blanes cells mediate persistent feedforward inhibition onto granule cells in the olfactory bulb. Neuron. 2006; 49:889–904. [PubMed: 16543136]

Rinberg D, Koulakov A, Gelperin A. Speed-accuracy tradeoff in olfaction. Neuron. 2006; 51:351–358. [PubMed: 16880129]

Saglietti L, Dequidt C, Kamieniarz K, Rousset MC, Valnegri P, Thoumine O, Beretta F, Fagni L, Choquet D, Sala C, et al. Extracellular interactions between GluR2 and N-cadherin in spine regulation. Neuron. 2007; 54:461–477. [PubMed: 17481398]

Sassoe-Pognetto M, Ottersen OP. Organization of ionotropic glutamate receptors at dendrodendritic synapses in the rat olfactory bulb. J Neurosci. 2000; 20:2192–2201. [PubMed: 10704494]

Schaefer AT, Angelo K, Spors H, Margrie TW. Neuronal oscillations enhance stimulus discrimination by ensuring action potential precision. PLoS biology. 2006; 4:e163. [PubMed: 16689623]

Schaefer AT, Margrie TW. Spatiotemporal representations in the olfactory system. Trends Neurosci. 2007; 30:92–100. [PubMed: 17224191]

Schild D. Principles of odor coding and a neural network for odor discrimination. Biophys J. 1988; 54:1001–1011. [PubMed: 3233263]

Seeburg PH, Single F, Kuner T, Higuchi M, Sprengel R. Genetic manipulation of key determinants of ion flow in glutamate receptor channels in the mouse. Brain Res. 2001; 907:233–243. [PubMed: 11430906]

Shepherd GM, Chen WR, Willhite D, Migliore M, Greer CA. The olfactory granule cell: from classical enigma to central role in olfactory processing. Brain Res Rev. 2007; 55:373–382. [PubMed: 17434592]

Shepherd, GM, Greer, CA. Olfactory bulbSynaptic organization of the brain. New York: Oxford University Press; 1990. 133–169.

Shimshek DR, Bus T, Grinevich V, Single FN, Mack V, Sprengel R, Spergel DJ, Seeburg PH. Impaired reproductive behavior by lack of GluR-B containing AMPA receptors but not of NMDA receptors in hypothalamic and septal neurons. Mol Endocrinol. 2006; 20:219–231. [PubMed: 16099814]

Shimshek DR, Bus T, Kim J, Mihaljevic A, Mack V, Seeburg PH, Sprengel R, Schaefer AT. Enhanced odor discrimination and impaired olfactory memory by spatially controlled switch of AMPA receptors. PLoS Biol. 2005; 3:e354. [PubMed: 16216087]

Spors H, Grinvald A. Spatio-temporal dynamics of odor representations in the mammalian olfactory bulb. Neuron. 2002; 34:301–315. [PubMed: 11970871]

Tang W, Ehrlich I, Wolff SB, Michalski AM, Wolfl S, Hasan MT, Luthi A, Sprengel R. Faithful expression of multiple proteins via 2A-peptide self-processing: a versatile and reliable method for manipulating brain circuits. J Neurosci. 2009; 29:8621–8629. [PubMed: 19587267]

Uchida N, Mainen ZF. Speed and accuracy of olfactory discrimination in the rat. Nat Neurosci. 2003; 6:1224–1229. [PubMed: 14566341]

Urban NN. Lateral inhibition in the olfactory bulb and in olfaction. Physiology & behavior. 2002; 77:607–612. [PubMed: 12527007]

Wellis DP, Kauer JS. GABAA and glutamate receptor involvement in dendrodendritic synaptic interactions from salamander olfactory bulb. The Journal of physiology. 1993; 469:315–339. [PubMed: 7903696]

Wellis DP, Kauer JS. GABAergic and glutamatergic synaptic input to identified granule cells in salamander olfactory bulb. The Journal of physiology. 1994; 475:419–430. [PubMed: 8006826]

Wimmer VC, Nevian T, Kuner T. Targeted in vivo expression of proteins in the calyx of Held. Pflugers Arch. 2004; 449:319–333. [PubMed: 15452710]

Yokoi M, Mori K, Nakanishi S. Refinement of odor molecule tuning by dendrodendritic synaptic inhibition in the olfactory bulb. Proc Natl Acad Sci U S A. 1995; 92:3371–3375. [PubMed: 7724568]

Europe PMC Funders Author Manuscripts

Europe PMC Funders Author Manuscripts

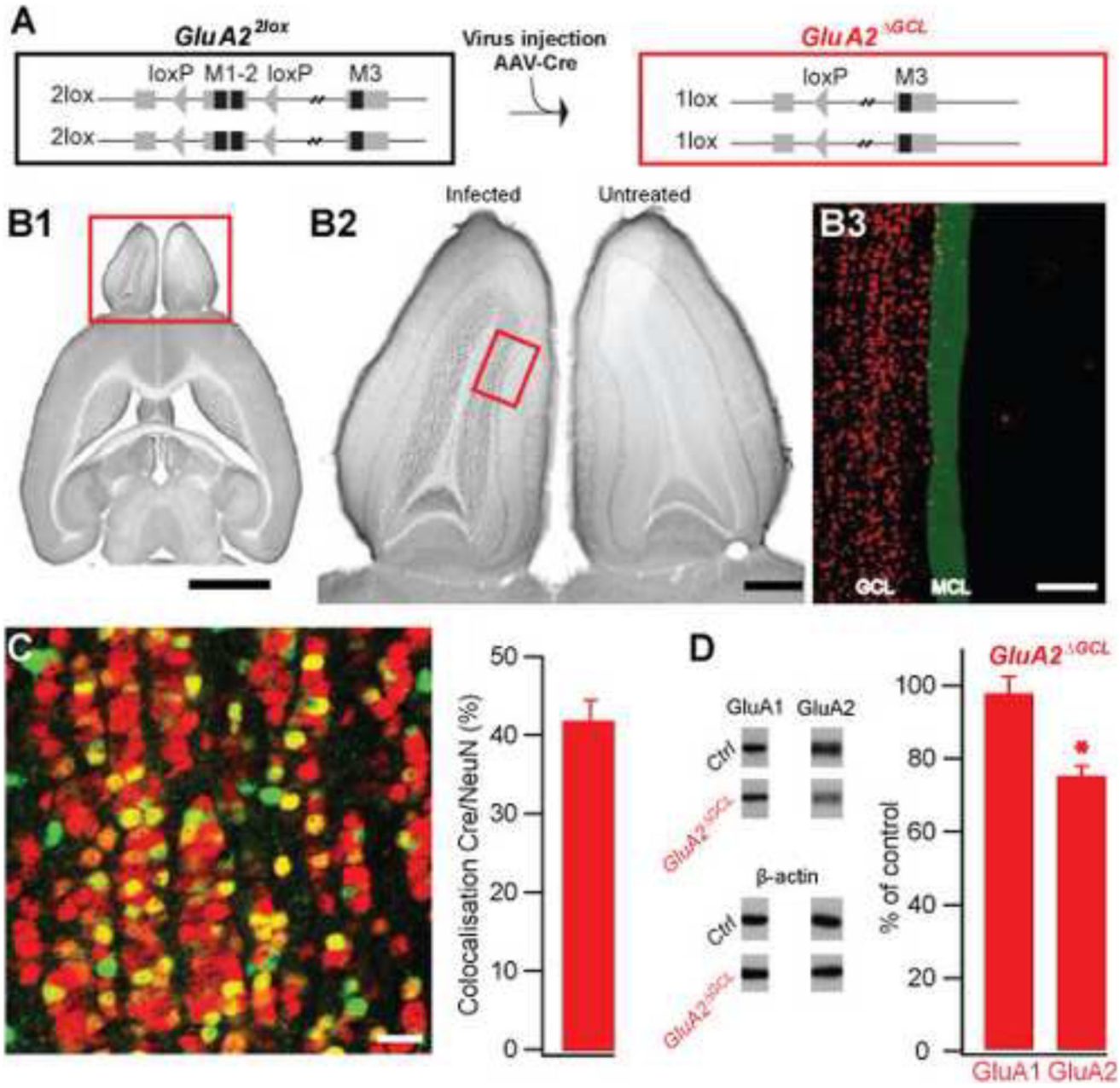

Figure 1. OB-specific GluA2 deletion.

A. Cre-mediated ablation of loxP-flanked transmembrane regions 1 and 2 of the GluA2 gene (M1-2, Exon 11, *GluA2*^{2lox}) by AAV-mediated Cre-expression in the GC layer of the OB (*GluA2*$^{\Delta GCL}$).

B. Specific AAV-mediated expression of Cre recombinase in the granule cell layer (GCL) of the left OB. B1, immuno-detection of Cre recombinase in the OB in comparison to the whole brain (DAB-stained transverse section). Scale bar 2.5 mm. B2, Cre expression in the left OB compared with a non-injected right side. Scale bar 0.5 mm. B3, Illustration of localization of Cre-positive cells (red) in the GCL relative to the mitral cell layer (MCL,

green). Cre-positive cells were derived by tresholding and MCL position was drawn manually. Scale bar 100 μm. Box in B1 indicates localization of higher magnification in B2, box in B2 shows an example for localization of image shown in B3.

C. Immunofluorescence overlay showing colocalization of Cre (green) and NeuN (red) in the GCL. Neurons expressing Cre appear in tones of yellow and orange, neurons not expressing Cre are red, and non-neuronal cells expressing Cre are green. Fraction of GCs expressing Cre: 42 ± 3 % (mean±SEM, n=14 samples, taken from 7 AAV-Cre infected mice). Because GCs undergo constant turnover, the fraction of infected cells is likely to be higher at the beginning of the experiment. Scale bar 20 μm.

D. Immunoblots of AAV-Cre infected (n=7) and non-infected (n=7) whole OB protein detecting GluA1 and GluA2, with β-actin as a loading control. GluA1 levels were unchanged compared to control (97±5%, mean ± SEM, n=39 samples, $p=0.6$), while the amount of GluA2 protein was significantly reduced (74±8%, mean±SEM, n=103 samples, $p<0.001$, student-*t* test).

Europe PMC Funders Author Manuscripts

Europe PMC Funders Author Manuscripts

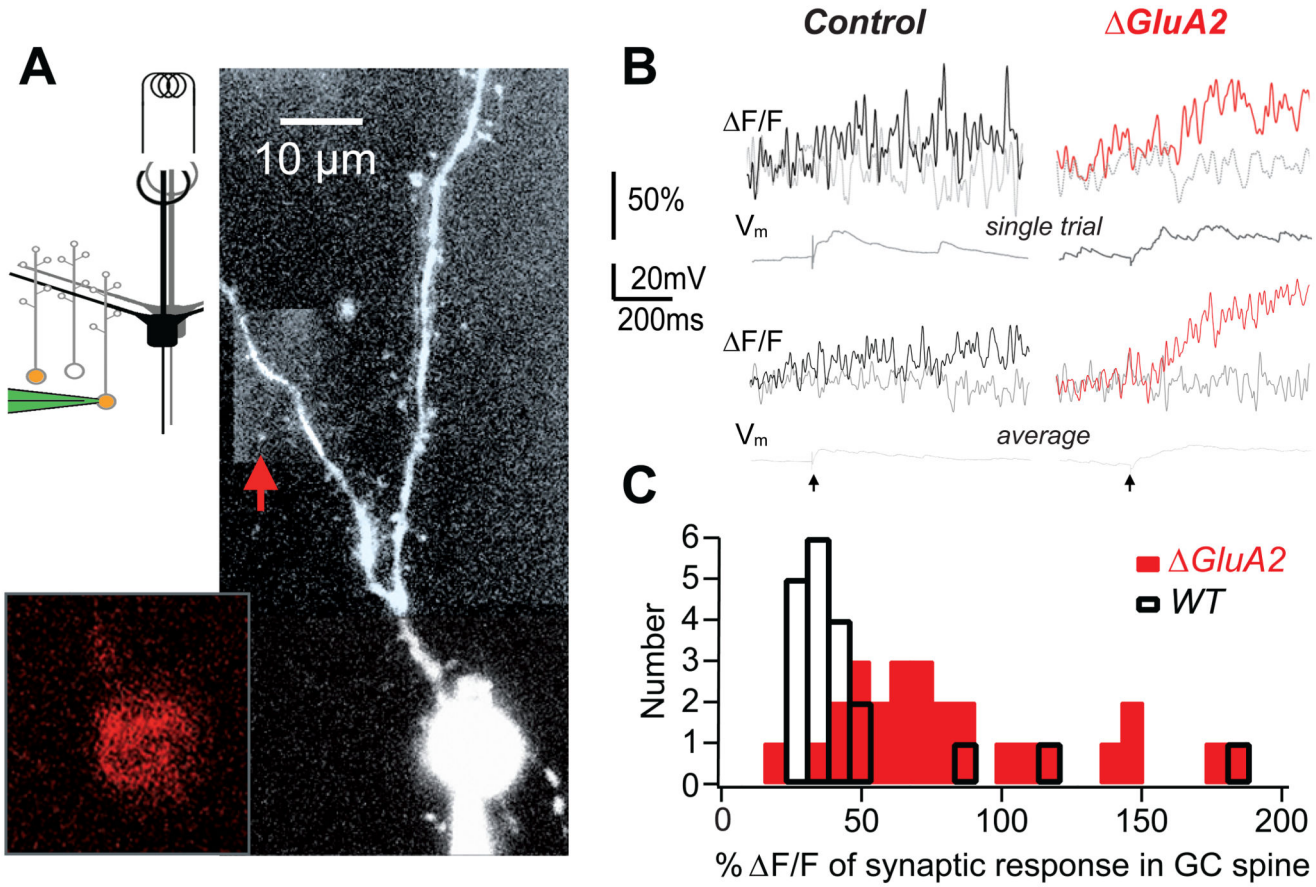

Figure 2. Increased Ca^{2+} inflow into granule cells lacking *GluA2*

A. Scheme showing recording configuration (red-filled GCs represent virally labeled GC, patch pipette (green), mitral cells (black/grey) and electrical stimulation at GL). Image shows GC of a P36 *GluA2*$^{\Delta GCL}$ mouse imaged with two-photon microscopy. In this case, AAV-Cre-2A-Kusabira Orange was used to express Cre recombinase and Kusabira Orange simultaneously, facilitating targeted patch-clamp recordings from GCs lacking GluA2. Granule cells were filled with 100 µM OGB-1 (signal in large panel) after identification of Kusabira Orange expression in the soma (inset, red).

B. Top panel: Individual synaptic fluorescence transients (ΔF/F) recorded from the spine (thick trace) and its adjacent dendrite (grey trace) marked by a red arrow in A. Corresponding voltage traces shown directly beneath. Lower panel: Averaged fluorescence and voltage signals (n=3 (cntrl), n=13 (ΔGluA2)). Stimulation artifact marked at the bottom.

C. Histograms of the amplitudes of individual synaptic responses in mouse GCs with unperturbed GluA2 (black; n = 20 events) and GluA2 deletion (red; n = 27 events).

Europe PMC Funders Author Manuscripts

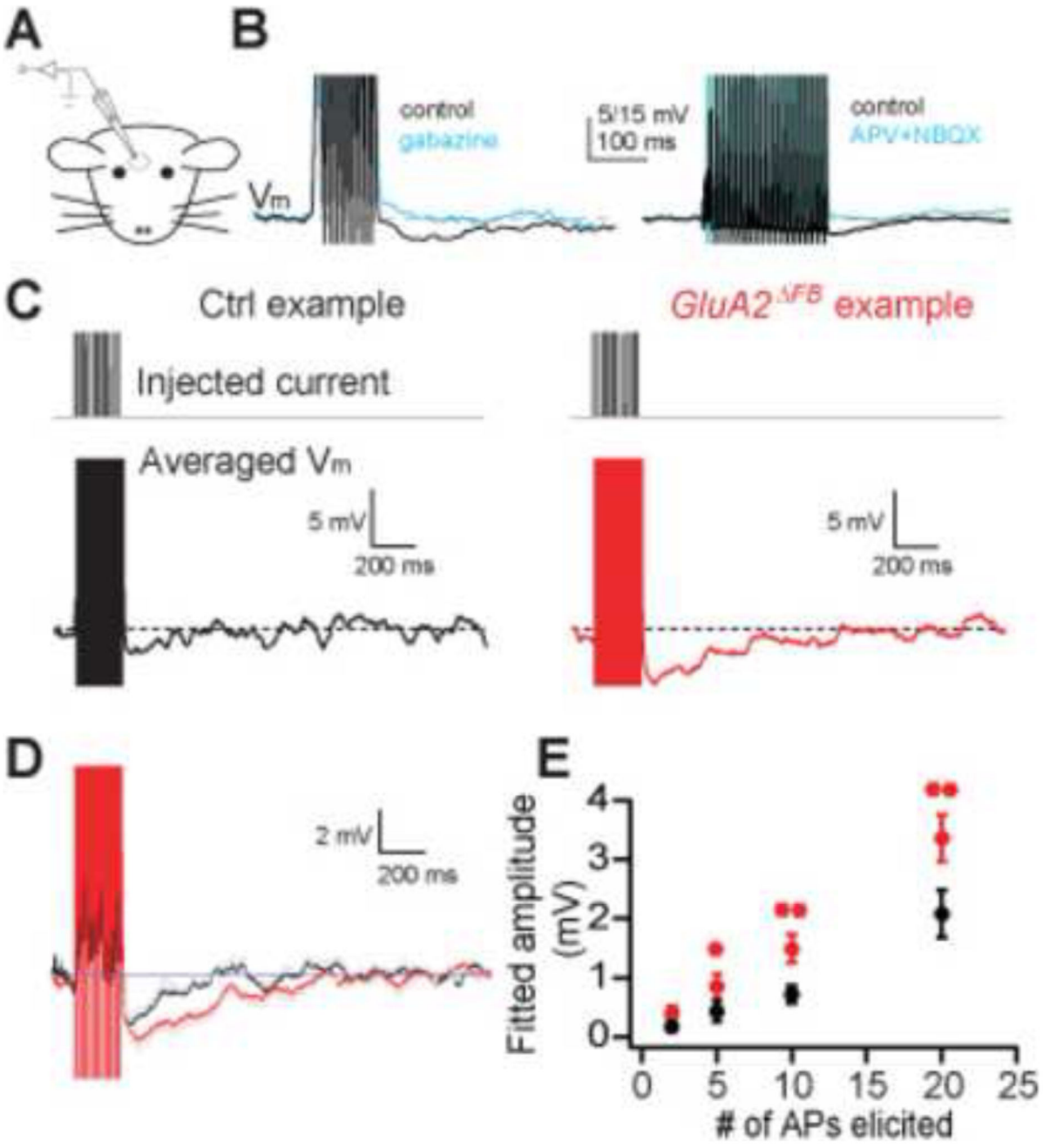

Figure 3. GluA2 deletion results in increased recurrent inhibition *in vivo*

A. Scheme of *in vivo* patch-clamp recordings from mitral cells in the OB.

B. Examples of *in vivo* patch-clamp recordings from mitral cells and stimulus paradigms used. Recurrent IPSPs were evoked by eliciting 10 or 20 APs and were blocked by application of blockers of GABAergic (500 μM Gabazine, left) or glutamatergic (500 μM APV and 500 μM NBQX, right) synaptic transmission.

C. Examples of *in vivo* patch-clamp recordings from a mitral cell in control (left) and *GluA2*$^{\Delta FB}$ (right) mice. 20 APs were evoked and traces were averaged as described in the supplementary information.

D. Averaged recurrent IPSP traces from n=9 cells (control) and n=15 cells (*GluA2*$^{\Delta FB}$) recorded from as shown in B. Gray lines indicate SEM between cells.

E. IPSP amplitude is proportional to stimulus strength and stronger in mitral cells of *GluA2*$^{\Delta FB}$ mice (**p<0.005, * p<0.05, 1-tailed t-test).

Europe PMC Funders Author Manuscripts

Europe PMC Funders Author Manuscripts

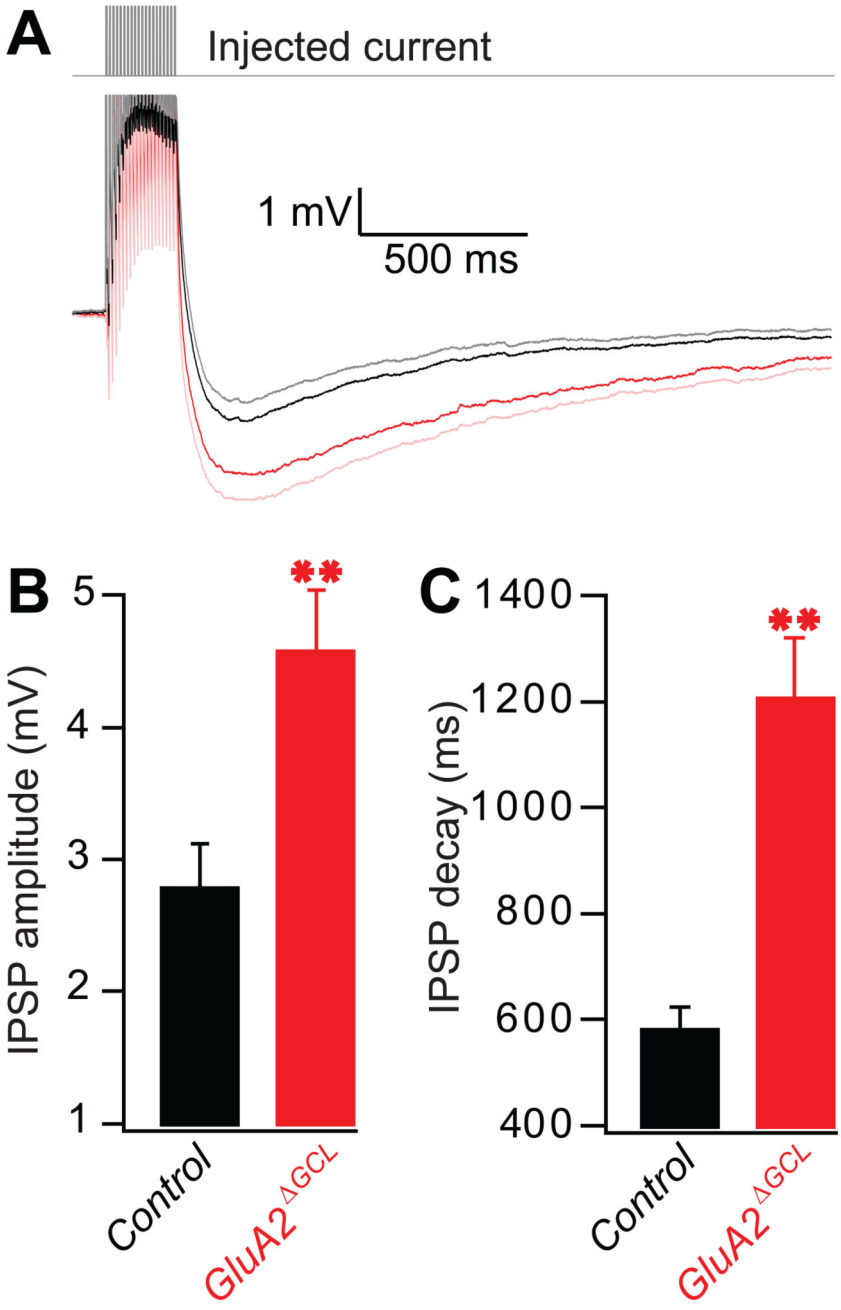

Figure 4. GluA2 deletion results in increased recurrent inhibition *in vitro*

A. Responses of mitral cells in OB slices from control (black) and *GluA2*$^{\Delta GCL}$ (red) elicited by 20 APs. Averaged traces of 11 control cells (C57BL6 and GluA2 littermate controls) and 13 *GluA2*$^{\Delta GCL}$ cells are shown with the SEM shown as grey and pink traces, respectively. B. Peak amplitudes of IPSPs (mean±SEM). The peak amplitude was determined within a 500 ms time window in each individual trace resulting in a higher mean as shown in A (2.76±0.35 mV, n=11 cells [C57BL6 and GluA2 littermate controls], 4.55±0.48 mV, n=13 cells [*GluA2*$^{\Delta GCL}$], p<0.01, Mann-Whitney).

C. Decay time constants of IPSPs (mean±SEM): 575±47 ms, n=11 cells [C57BL6 and GluA2 littermate controls], 1199±120 ms, n=13 cells [$GluA2^{\Delta GCL}$], p=<0.0001, t-test.

Europe PMC Funders Author Manuscripts

Europe PMC Funders Author Manuscripts

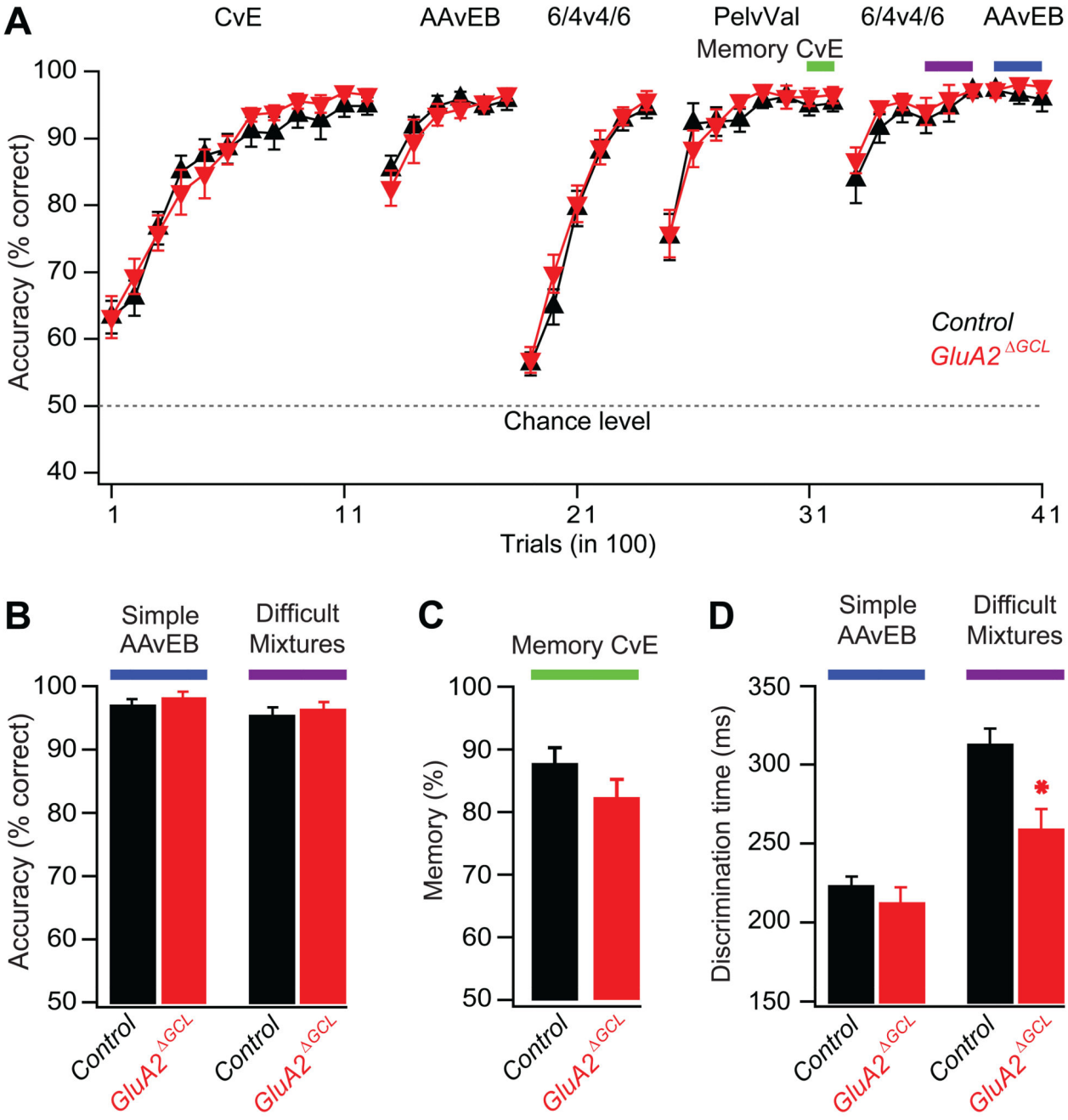

Figure 5. OB-specific GluA2 deletion accelerates discrimination of similar odors and does not affect learning and memory

A. Accuracy shown as the percentage of correct choices for simple odor pairs (each 1% in mineral oil): cineol (C), eugenol (E), amyl acetate (AA), ethyl butyrate (EB), pelargonic acid (Pel), valeric acid (Val). Difficult mixture: 0.4% AA/0.6% EB versus 0.6% AA/0.4% EB. Colored bars depict trials taken for quantitative analyses in panels B to D. Learning performance was indistinguishable between the groups (ANOVA, $F = 0.85$, $p = 0.4$).

B. Accuracy (mean ± SEM). No difference was observed in performance levels of *GluA2*$^{\Delta GCL}$ (98±1%, n=11) and control mice (97±1%, n=13) for simple odors (p=0.4,

Mann-Whitney) and similar odor mixtures (*GluA2*$^{\Delta GCL}$ 96±2%, n=11, control mice, 95±2%, n=13 p=0.5, Mann-Whitney). The two groups of control mice were pooled. C. Memory (mean ± SEM) after two weeks for cineol versus eugenol in *GluA2*$^{\Delta GCL}$ (red bar, n=11) and control (black bar, n=13) mice was indistinguishable (p=0.3, student-*t* test). D. Discrimination time (mean ± SEM). *GluA2*$^{\Delta GCL}$ (211.7±10.9 ms, n=11) and control mice (222.5±6.8 ms, n=13) did not differ significantly for simple odors (p=0.4, student-*t* test), but discrimination time was substantially reduced for similar odor mixtures when comparing *GluA2*$^{\Delta GCL}$ (257.1±15.2 ms, n=11) with control mice (311.1±11.8 ms, n=13 p<0.01, student-*t* test).

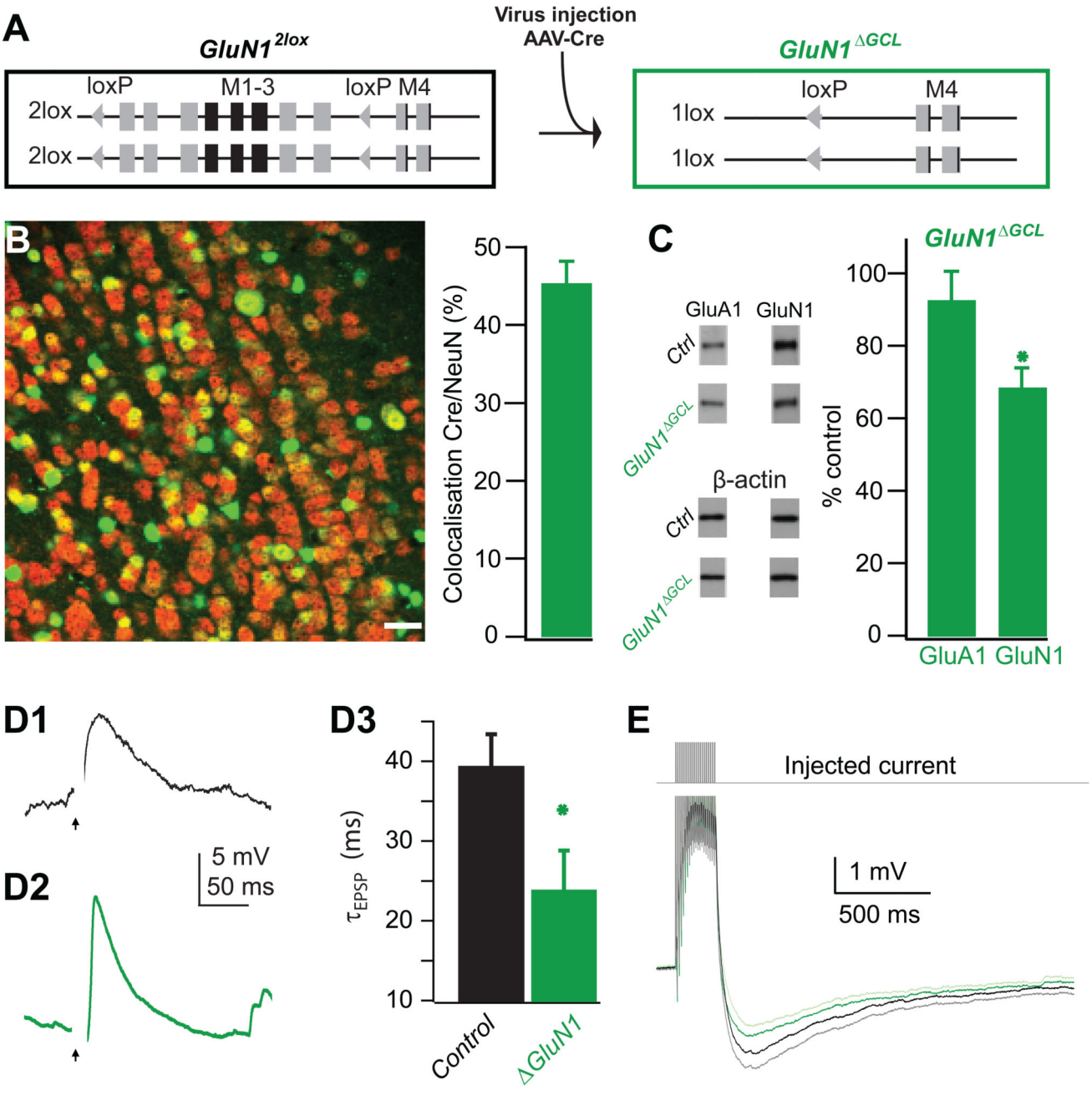

Figure 6. OB-specific GluN1 deletion

A. AAV-Cre-mediated ablation of loxP-flanked transmembrane regions 1, 2 and 3 of the GluN1 gene (M1-3, Exons 11-18, *GluN1*^{2lox}) by AAV-mediated Cre-expression in the granule layer of the OB (*GluN1*$^{\Delta GCL}$).

B. Immunofluorescence detection of Cre in the OB (see also legend to Figure 1C). The fraction of GCs expressing Cre was 45 ± 3 % (mean±SEM, n=9 samples, taken from 2 AAV-Cre infected mice). Scale bar 20 μm.

C. Quantification of immunoblots of AAV-Cre infected (n=2) and non-infected (n=6) whole OB protein detecting GluA1, GluN1 and β-actin. GluA1 levels were unchanged compared to control (92±8%, mean±SEM, n=11 samples p=0.3), while the amount of GluN1 protein was significantly reduced (68±6%, mean±SEM, n=22 samples, p<0.001, student-*t* test).
D. *In vitro* whole-cell recording of evoked EPSPs in uninfected GC (D1) and GC with GluN1-deletion (D2). Time of glomerular stimulation marked by arrowhead; stimulus artifact is blanked; membrane potential approximately -80 mV, see text for details). (D3) Quantification of decay kinetics (values see main text).
E. Responses of mitral cells in OB slices from control (black) and $GluN1^{\Delta GCL}$ (green) elicited by 20 APs. Averaged traces of 11 control cells (C57BL6 and GluA2 littermate controls) and 14 $GluN1^{\Delta GCL}$ cells are shown with the SEM shown as grey and light green traces, respectively.

Europe PMC Funders Author Manuscripts

Europe PMC Funders Author Manuscripts

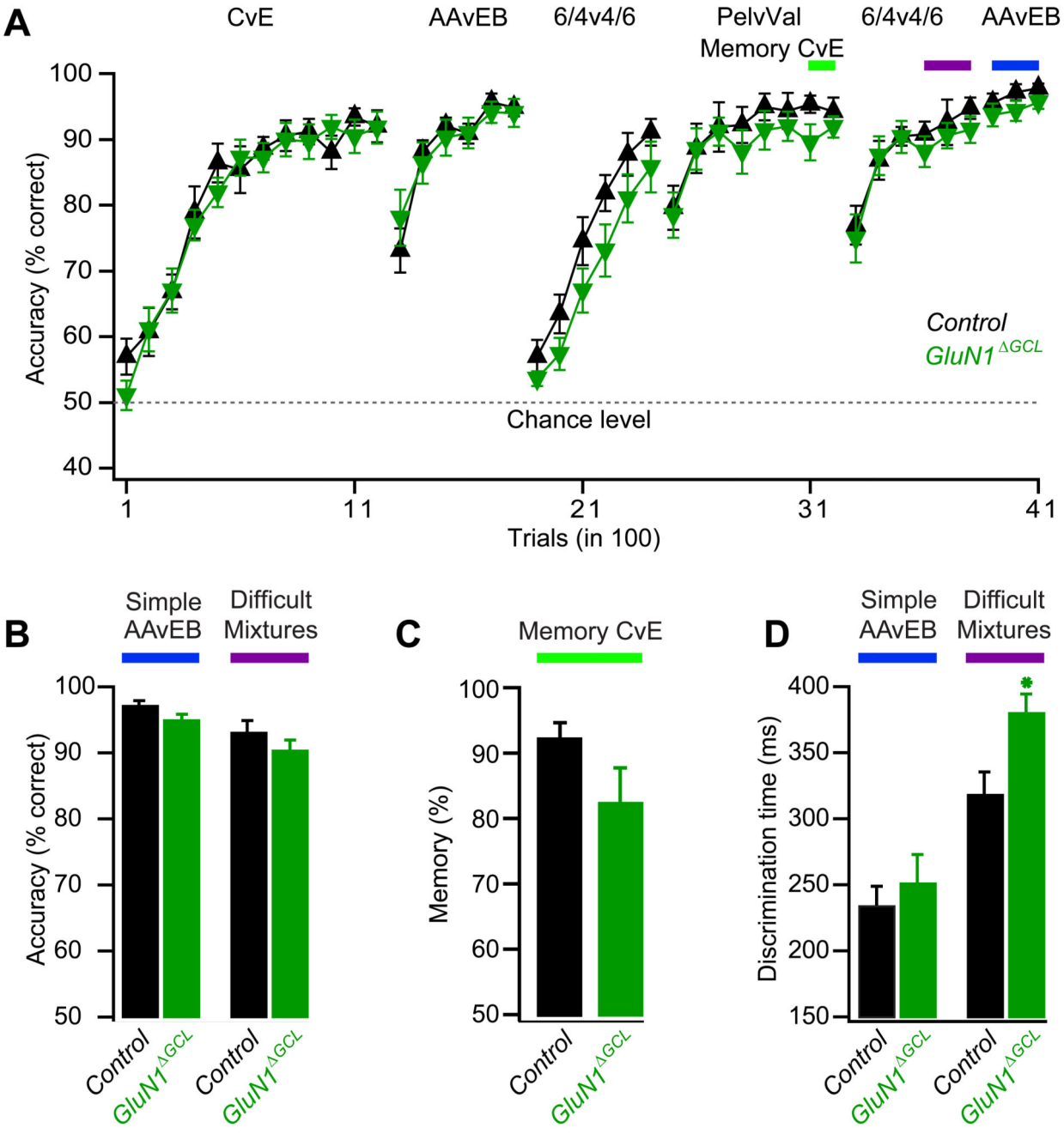

Figure 7. OB-specific GluN1 deletion slows discrimination of similar odors and does not affect learning and memory

A. Learning curves as in Fig. 5A.

B. Accuracy shown as the percentage of correct choices (mean ± SEM). No difference observed in performance levels of *GluN1*$^{\Delta GCL}$ (94.6±1%, n=10) and control mice (96.8±1%, n=9) for simple odors (p=0.2, student-*t* test) and similar odor mixtures (*GluN1*$^{\Delta GCL}$ (90±1.8%, n=10, Control mice, 92.7±2.1%, n=9, p=0.4, student-*t* test).

C. Memory (mean ± SEM) after two weeks for cineol versus eugenol in *GluN1*$^{\Delta GCL}$ mice (red bar, n=10) and control (black bar, n=9) mice was not significantly different (p=0.1, student-*t* test).

D. Discrimination time (mean ± SEM). *GluN1*$^{\Delta GCL}$ (249.3±22.6 ms, n=10) and control mice (232.1±15.9 ms, n=9) did not differ significantly for simple odors (p=0.5, student-*t* test), but discrimination time was significantly increased for similar odor mixtures when comparing *GluN1*$^{\Delta GCL}$ (378.3±15.4 ms, n=10) with control mice (316.2±18.4 ms, n=9, $p<0.05$, student-*t* test).

Europe PMC Funders Author Manuscripts

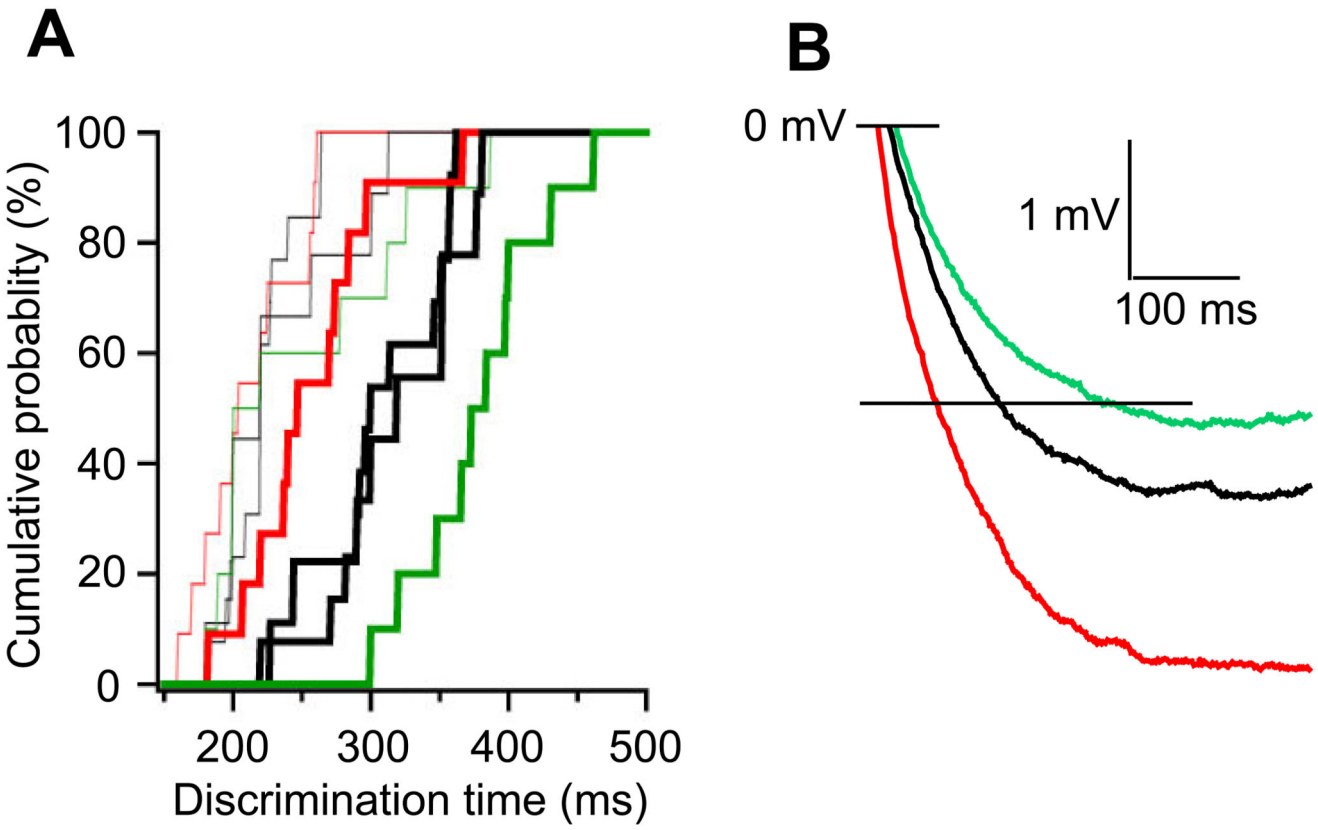

Figure 8. Bidirectional shifts of odor discrimination time

A. Cumulative probabilities of odor discrimination times for simple odors (thin lines) and mixtures (thick lines). Discrimination times determined for controls (black, both from Fig. 5 and Fig. 7), *GluA2*$^{\Delta GCL}$ (red) and *GluN1*$^{\Delta GCL}$ (green) mice.

B. Dendrodendritic inhibition. Averaged traces of control (black), *GluA2*$^{\Delta GCL}$ (red) and *GluN1*$^{\Delta GCL}$ (green) shown in Figs. 4A and 7E1.